Colors for figures : For a proper readability of the figures, all require color printing.

Graphical Abstract

Oxidation kinetics of a rough laminar pyrocarbon in O_2-, H_2O- and CO_2-containing atmospheres*

Marina Fradin, Gérard L. Vignoles, Charlotte Ville, Guillaume Couégnat, Mathilde Ridard, Francis Rebillat

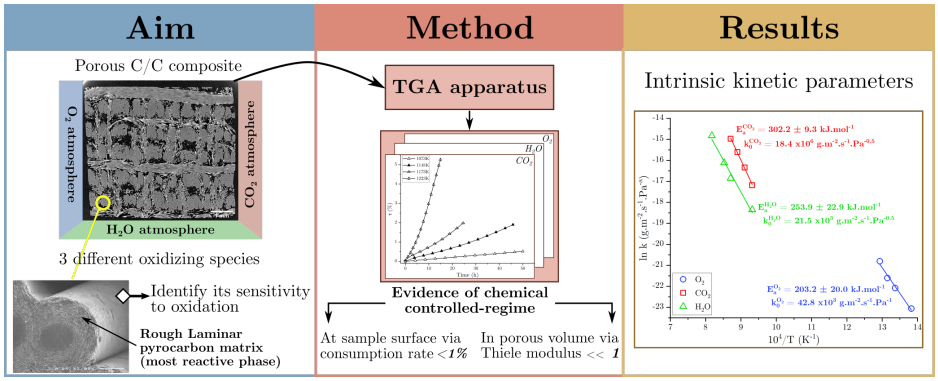

Highlights

Oxidation kinetics of a rough laminar pyrocarbon in O_2-, H_2O- and CO_2-containing atmospheres

Marina Fradin, Gérard L. Vignoles, Charlotte Ville, Guillaume Couégnat, Mathilde Ridard, Francis Rebillat

- oxidation of a porous C/C composite under O_2, H_2O and CO_2 atmospheres ;
- matrix surface highly developed and exposed is the dominant reacting phase ;
- X-ray micro-tomography imaging and correlation technique characterizations ;
- oxidation chemical regime occurs in the porous volume and at the surface ;
- identification of intrinsic oxidation kinetics for a rough laminar pyrocarbon.

Oxidation kinetics of a rough laminar pyrocarbon in O_2-, H_2O- and CO_2-containing atmospheres

Marina Fradin[a,b,*], Gérard L. Vignoles[a], Charlotte Ville[a], Guillaume Couégnat[a], Mathilde Ridard[b], Francis Rebillat[a]

[a] *Laboratoire des Composites ThermoStructuraux (LCTS), UMR 5801 CNRS-Safran-CEA-Université de Bordeaux, 3 Allée de La Boétie, 33600 Pessac, France*
[b] *ArianeGroup SAS, 3 Rue de Touban, 33185 Le Haillan, France*

Abstract

The originality of this work relies on the identification of kinetic parameters for a rough laminar pyrocarbon material under three different oxidizing atmospheres. Thermogravimetric analysis was used to carry out oxidation tests on a ex-CVI porous C/C composite under O_2-, H_2O- and CO_2-containing atmospheres at ≪ low-temperatures ≫. They were proven to be in a chemical reaction-controlled regime in the porous volume of the material and at its external surface through the use of X-rays micro-tomography characterization technique and simple analytical model-based considerations. Activation energies of 203.2 kJ.mol^{-1}, 253.9 kJ.mol^{-1} and 302.2 kJ.mol^{-1} were identified under O_2, H_2O and CO_2.

Keywords: C. oxidation, C. kinetic parameters, A. ceramic matrix composites, A. carbon, B. 3D computed tomography, B. SEM.

1. Introduction

Carbon/Carbon (C/C) composites feature attractive properties, such as light weight, stability to high temperatures, huge specific strength, low thermal expansion coefficient, explaining their wide use as nozzle throat parts, re-entry vehicle thermal protections, and airplane brake disks for instance [1, 2, 3, 4, 5, 6].

⋆. Working document - not for public release.
∗. Corresponding author. Tel : (+33) 5 56 84 33 03.
Email address: fradin@lcts.u-bordeaux.fr (Marina Fradin)

In these types of applications, C/C composites are exposed to high temperatures and chemical environments containing oxidizing species such as H_2O, CO_2 and O_2, eventually leading to an ablation phenomenon and a non-negligible surface etching [7, 8, 9]. Graphite-like materials are well known to start degrading at 673K under dioxygen and at 973K under H_2O and CO_2-containing atmospheres [10, 11]. Therefore, their kinetic behavior in specific oxidizing conditions has to be known in order to anticipate and precisely quantify the material degradation. The behavior of C/C composites under various oxidizing atmospheres has been studied during the last fifty years considering different parameters : recession rate, effective reactivity, roughness and morphologies, topological evolutions, either by experiments or modeling [7, 12, 13, 14, 15]. However, the leading role in these complex phenomena is held by the intrinsic kinetics of each of the carbonaceous phases in presence. Their identification still remains challenging.

In the last few years, several experimental and numerical studies, that must be mentioned, tackled the problem of identifying intrinsic kinetics of miscellaneous carbon materials, inbred or processed, under O_2 or H_2O or CO_2 atmospheres. Smith [16] collected oxidation data from various carbonaceous materials under dry air at temperatures from 580K to 2200K and determined overall kinetics parameters. The behavior of an ex-pitch matrix and an ex-Chemical Vapor Deposition (CVD) matrix under dry air were respectively studied by Drawin *et al.* [17] and Luo *et al.* [18]. The behavior of carbon particles under water vapour, among other complex atmospheres, was studied by Libby and Blake [19] at high temperatures using computational methods. Bradley *et al.* [20] identified heterogeneous oxidation kinetics for solid graphite particles under O_2, H_2O and CO_2. Bertran *et al.* [21] determined kinetics parameters for an ex-resin type matrix under dry air and water vapor at temperatures between 623K and 773K. Besides, Qin *et al.* [22] identified kinetics constants for an ex-pitch matrix and for ex-PAN fibers under water vapor at 873 to 1673K. Golovina [23] studied the gasification of a graphite material under a CO_2 atmosphere at very high temperatures between 1600K and 2600K. The behavior of highly graphitized spectroscopic graphite powders under a CO_2 atmosphere at temperatures bet-

ween 973K and 1373K was evaluated by McKee *et al.* [24, 25]. Ergun [26] studied the behavior of different types of carbons (Ceylon graphite, activated carbon, and activated graphite) under a CO_2 atmosphere between 973K and 1773K.

Carbonaceous materials oxidation under O_2, H_2O and CO_2 was also studied considering the energies of the adsorption step of the reactants and desorption step of $CO_{(g)}$ as a product from the surface of different carbon materials. Rossberg [27] suggested that the slow and determining step is the dissociation of an oxygen atom to the active carbon site and compared the dissocation energy to the true activation energies of the reaction. For spectroscopic carbons oxidized at temperatures from 793K to 1693K under O_2, a dissociation energy of 246.9 kJ.mol^{-1} was found, one of 485.3 kJ.mol^{-1} under H_2O, and finally one of 527.2 kJ.mol^{-1} under CO_2. Kelemen and Freund [28] found an energy of 133 and 209 to 251 kJ.mol^{-1} for the adsorption step of O_2 and CO_2 respectively on glassy carbons at 573K. Karlström *et al.* [29] studying biomass char proved that the adsorption step of O_2, H_2O and CO_2 on $C_{(s)}$ atoms differ by their activation energies with reported values of 1, 223 and 226 kJ.mol^{-1} respectively. On the other hand, they found activation energies for the desorption step of $CO_{(g)}$ of 1, 192 and 234 kJ.mol^{-1}.

In a nutshell, oxidation kinetics data under O_2, or H_2O or CO_2 oxidizing atmospheres are really dispersed because of the different natures of the carbonaceous materials studied in terms of graphitic structure and reactivity. This highlights the fact that the behavior of each carbonaceous material under specific oxidizing conditions has to be precisely studied and cannot be inferred from an another material without a loss of accuracy. Besides, this short bibliographical review underlines that there is a lack of oxidation kinetics data for pyrocarbon (PyC) materials in literature. On the other hand, oxidation kinetics data of one specific carbon material under three different oxidative atmospheres are scarce, except the work of Bradley *et al.* [20] on graphite particles which are highly organized materials, and the adsorption-desorption considerations of reactants and CO-product from Rossberg [27] and Karlström *et al.* [29] which constitute for most of them very longstanding experimental studies. Those kinds of works are even

scarcer, if not inexistent, for PyC materials.

In this work, we are aiming at investigating the oxidation kinetic behavior of a Rough Laminar (RL) PyC matrix under O_2, H_2O and CO_2-containing atmospheres. RL pyrocarbon is a very important material in space technology but unavailable in bulk form, making the determination of its intrinsic reactivity extremely difficult. Indeed, RL PyC is only produced by Chemical Vapor Infiltration (CVI) [30, 31, 32, 33] inside porous media developing a large internal surface area and with a very specific set of processing parameters [34].

To do so, the material under consideration is a 3D needle-punched highly porous C/C composite, in which the raw fibrous architecture has been covered in volume with an RL PyC matrix by CVI. Hence, the matrix represents the only and most widespread surface in the porous volume of the material. The fibers, less directly exposed to the oxidizing gases, are also far less reactive to oxidation than the matrix due to their intrinsic characteristics. It is therefore possible to assume that oxidation affects the matrix only. The phenomenon of competition between reaction and diffusion during the oxidation process of carbon materials and C/C composites has been extensively reported in the literature to misrepresent the kinetic behavior of the material when oxidation is limited by the diffusion of the oxidizing species to the carbon surface [9, 10, 14, 35, 36, 37, 38, 39]. For that reason, a complete chemical-controlled regime freed from diffusion effects in the porous volume of the material is targeted in this study. So that, the identified kinetics related to the oxidation of the matrix, which occupies the overall developed surface in the porous volume of the material, could be defined as intrinsic.

The methodology to determine intrinsic oxidation kinetics for the RL PyC matrix followed in this study thus contains several experimental and validation steps. Oxidation tests are carried out in a Thermogravimetric Analysis (TGA) apparatus and kinetics parameters are extracted from mass loss results. Surface and volumic oxidation morphologies are analyzed using a 3D-image characterization technique and Scanning Electron Microscopy (SEM) imaging. The existence of the targeted chemical regime at the sample surface and in its porous volume is verified using experimental and analytical modeling considerations.

Finally, comparisons of the identified kinetics parameters with literature data are discussed.

2. Materials and Methods

2.1. Materials

The oxidation behavior of a partly infiltrated 3D needle-punched C/C composite is investigated in this study. The preform is made of carbon yarn sheets of ex-PAN fibers, horizontally and perpendicularly stacked (X, Y planes), then needle-punched in the transverse direction (Z) to hold them together. Fig. 1 gives an illustration of the architecture. Its porosity is estimated at 28% ± 2% [40, 41]. The fabrication process of the ex-PAN fibers is conventional, as described in the work of Frank *et al.* [42]. The Isobaric and Isothermal CVI process (I-CVI) is used to fill the preform with a pyrocarbon matrix until a solid matrix fraction of 35 ± 3%, a residual porosity of 37 ± 2% and an apparent density of 1.25 ± 0.1 g.cm^{-3} are reached.

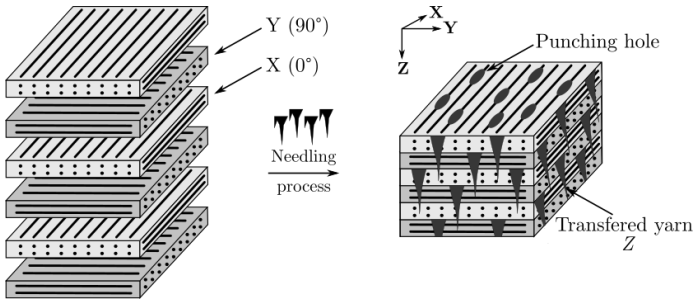

FIGURE 1 – Schematic illustration of the 3D needle-punched C/C architecture.

The overall organization of the material is displayed on Fig. 2 through X-ray micro-tomography and SEM images and the types of pores constituting the porous volume of the material are indicated. The pores size associated to this type of C/C composites is different from the IUPAC format and is given as

follows : pores sizes ranging from 200 to 1000 µm are inter-plies macroscopic pores, ones between from 10 to 200 µm are mesoscopic inter-yarns pores and the ones below 10 µm are intra-yarn microscopic pores [43].

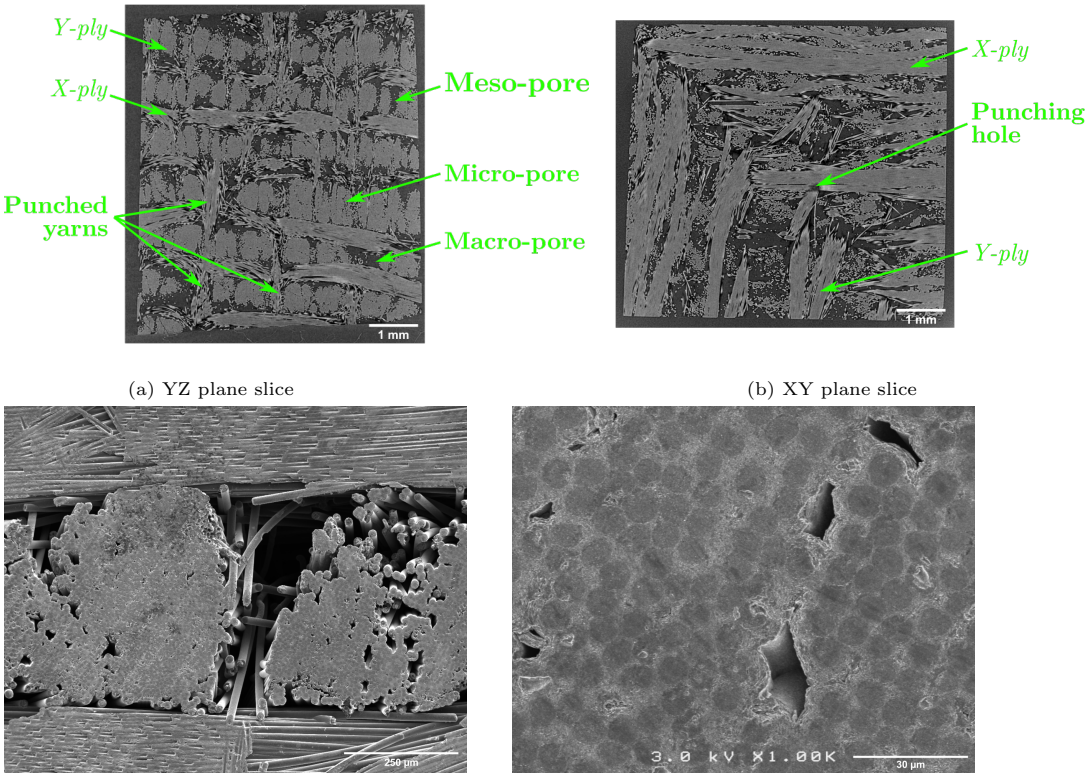

(a) YZ plane slice

(b) XY plane slice

(c) Yarns and inter-yarns pore

(d) Tip of a yarn and intra-yarn pores

FIGURE 2 – Vizulaisation of the organization of the material at different scale. (a, b) Core slices of X-ray micro-tomography of the porous C/C sample according to the (a) YZ-plane and (b) XY-plane. (c, d) SEM images of (c) the inter-yarns area and (d) the tip of a yarn.

2.2. Sample preparation

Cubic samples of 6 mm edge size are used. They have been previously cut with a wire saw in a C/C massive block. Faces were polished on silicon carbide

discs in order to standardize the dimensions.

2.3. Characterization of the carbon textures

An optical microscope Nikon ME600L equipped with a graduated polarizer and an analyzer is used to determine the fibers and matrix anisotropy. The extinction angle A_e is measured using the Polarized Light Optical Microscopy (PLOM) method established by Gillard *et al.* [44]. A LabRAM HR (Horiba-Jobin Yvon) Raman spectrometer with a wavelength of 632.8 nm is employed to assess the Full Width at Half Maximum of the D-band ($FWHM_D$), the Half Width at Half Maximum of the G-band ($HWHM_G$) and the ratio of the D-band intensity to the G-band intensity (I_D/I_G). These parameters are known to be related to the amount of in-plane defects and graphitization degree of pyrocarbons [45, 46, 47]. The in-plane coherence length L_a of the cristallites of the fibers and the matrix is undertaken using the method established by Mallet-Ladeira *et al.* [48] based on the $HWHM_G$ parameter.

2.4. Oxidation test equipment

The objective of this study is to assess the behavior of a porous C/C composite towards three different types of oxidizing species : *(1)* $O_{2(g)}$ associated to the reaction equation Eq. 1 in a dry air-like atmosphere mainly producing $CO_{2(g)}$, according to thermodynamical considerations under 973K [49, 50] ; *(2)* $H_2O_{(g)}$ related to Eq. 2 in a water vapour mix ; *(3)* CO_2 corresponding to Eq. 3.

$$C_{(s)} + O_{2(g)} \rightleftharpoons CO_{2(g)} \tag{1}$$

$$C_{(s)} + H_2O_{(g)} \rightleftharpoons CO_{(g)} + H_{2(g)} \tag{2}$$

$$C_{(s)} + CO_{2(g)} \rightleftharpoons 2CO_{(g)} \tag{3}$$

A SETARAM Setsys 1600 TGA reactor was used to carry out the oxidation experiments. The internal diameter of the cylindrical reaction chamber is 17.8

mm and it is surrounded by a cylindrical resistive heating. A highly accurate balance, with a precision as high as 1×10^{-5} g, is positioned at the top of the apparatus to measure sample weight loss during testing. A thermocouple sensor, located close to the sample, monitors the chamber temperature. Fig. 3 gives a schematic diagram of the complete experimental facility. Cubic samples were installed in an airy basket-like crucible made of alumina and platinum connected to the balance. They were oriented in a way that needle-punched fibers were pointing downwards.

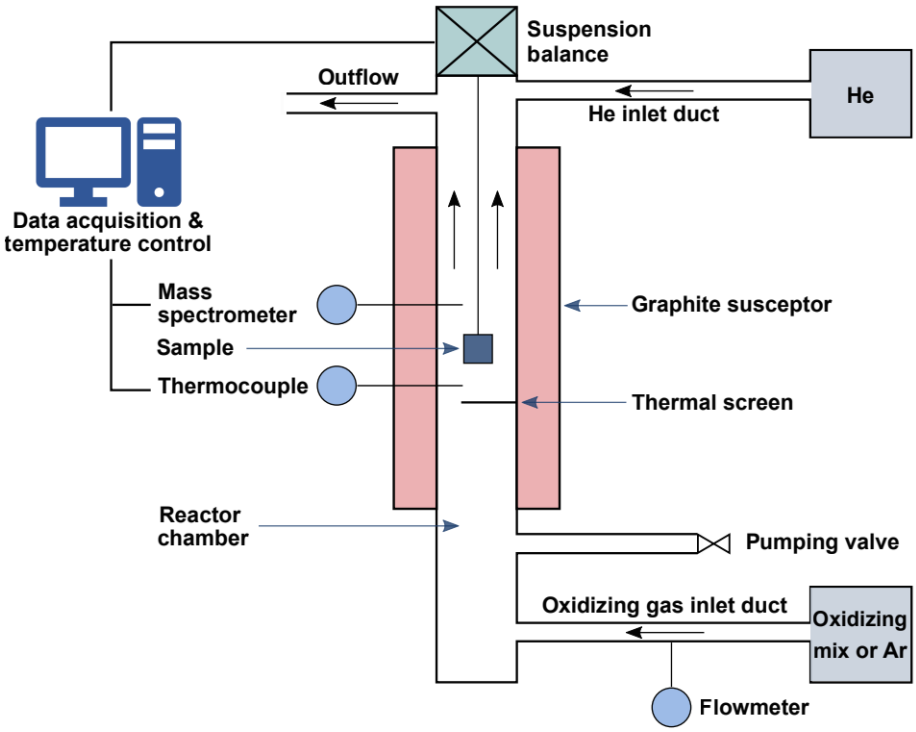

FIGURE 3 – Diagram of the TGA equipment.

The oxidizing atmospheres were produced by mixing each of the oxidizing species (O_2, H_2O or CO_2) with dinitrogen (N_2) in a 20%-80% proportion in partial pressure at standard conditions. The overall oxidizing gas flow was set to 2 $L.h^{-1}$ and injected from the bottom of the chamber.

Heating and cooling steps were carried out under a neutral atmosphere of argon. A 10 K.min^{-1} rate was used to reach the desired temperature. The oxidation process has been carried out under isostatic temperatures. The temperature range under each atmosphere is selected in such a way that the lowest temperature corresponds to the first temperature under which a mass loss is observed. The other temperatures of the range are selected to ensure the oxidation process stays in a chemical-controlled regime (see Section 3.4 for further details). The oxidizing bearing temperatures were : 723 to 773K for the dry air atmosphere ; 1073 to 1223K for the water vapour atmosphere ; and 1073 to 1148K for the CO_2 atmosphere, respectively.

2.5. Surface observations

The examination of the samples post-test surface morphologies, and especially the determination of the dominant reacting phase, was performed using a Hitachi S4500 FEG SEM. An electron beam voltage of 3 kV and a working distance of 15 mm were choosen.

2.6. Volumic characterizations

The evolutions of the material in its porous volume due to oxidation were tracked with an innovative approach relying on 3D X-ray computed microtomography (µCT) and image correlation. A laboratory tomograph (GE v|tome|x s research edition, General Electrics, USA) was used to acquire pre- and post-test images of the samples. The tomograph X-rays source was set on a tension of 100 kV and an intensity of 250 µA. The exposure time was 1000 ms. A total of 2000 images were acquired per scan. The spatial resolution was 4.75 µm per voxel unit.

Post-test images were then registered with respect to their pre-test reference state. The registration was performed using an in-house digital volume correlation software. The sought mapping is assumed to be described by a global affine transformation, including rigid translation and rotation of the specimen. It also

possibly includes a homothetic scaling to accommodate small variations in the images resolution. Also, prior to the registration, images are standardized to mitigate differences in brightness and contrast between specimens. The transformation parameters are found by minimizing the gray level residual between the mapped image and the reference one. A difference image is finally obtained by subtracting the registered image from the reference one using the *Image Calculator* function in *Fiji* software [51].

2.7. Data processing

The primary oxidation behavior with time is evaluated with the burn-off ratio τ (%) defined as the mass loss of the sample at a specific time compared to its initial mass m_0 (g) :

$$\tau = 1 - \frac{m_i}{m_0} \ \% \tag{4}$$

where m_i (g) is the sample mass at time i.
Then, the oxidation activity j (g.m^{-2}.s^{-1}) is calculated from Eq. 5, where $\dot{\tau}$ (%.s^{-1}) is the slope of the burn-off evolution curve in its linear part :

$$j = \dot{\tau} \ m_0 \ \frac{1}{S_{vol}} \tag{5}$$

S_{vol} (m^2) is the surface area developed by the matrix in the open volume of the porous C/C sample, satisfying the following equation :

$$S_{vol} = \sigma_v \ V_{geo} \tag{6}$$

where V_{geo} (m^3) is the geometric volume of a sample and σ_v (m^{-1}) is the internal surface area. For the C/C composite of this study, σ_v has been determined by X-ray µCT and image processing with a numerical method set by Charles *et al.* [52]. For a C/C composite featuring a porosity rate of 37%, it is equal to 24.6 $\times$ 10 ^{4} m^{-1}.

j also satisfies Eq. 7 :

$$j = k \ P_{ox}^a \tag{7}$$

where P_{ox} (Pa) is the partial pressure of the oxidizing species and is a the reaction partial order. It is commonly taken equal to 1 under O_2 [7, 21, 47, 16], and will be considered equal to 0.5 under H_2O and CO_2 [20, 22].

In Eq. 7, k ($g.m^{-2}.s^{-1}.Pa^{-a}$) is the oxidation reactivity and is assumed to satisfy an Arrhenius law as follows :

$$k = k_0 \; exp\left(\frac{-E_a}{\mathcal{R}T}\right) \tag{8}$$

where k_0 ($g.m^{-2}.s^{-1}.Pa^{-a}$) is the pre-exponential factor, E_a the reaction activation energy ($J.mol^{-1}$), $\mathcal{R}$ the universal ideal gas constant ($J.mol^{-1}.K^{-1}$) and T the reaction temperature (K).

Finally, the consumption ratio per geometrical surface unit, defined as the ratio between the number of carbon moles consumed and the amount of available oxidizing species per sample external surface unit, is expressed by ζ ($\%.mm^{-2}$) as follows :

$$\zeta = \frac{n_C^{cons.}}{n_{ox}^{avail.}} \frac{1}{S_{geo}} \tag{9}$$

where S_{geo} is the geometrical external surface of the sample (mm^2). The ratio between the number of carbon moles consumed and the amount of available oxidizing species ranges between 0% (*i.e.* no consumption) to 100% (*i.e.* complete consumption by the sample external surface). It might increase with temperature due to the kinetic activation. Consequently, for a 6 mm edge size cubic sample, ζ would go from $0\%.mm^{-2}$ to $4.16 \times 10^{-1}\%.mm^{-2}$.

3. Results and discussion

3.1. Fibers and matrix textures and structures

Fibers and matrix being different types of materials, their textures and structures features need to be characterized first. Table 1 summarizes the pyrolytic texture and structure characteristics of the fibers and the matrix phases assessed with the methods described in Section 2.3. With a very low extinction angle,

the fibers displayed a characteristic transversely isotropic texture of ex-PAN materials [53]. Coupled data from PLOM and Raman indicate that the matrix is indeed an RL PyC [44]. With a larger $FWHM_D$ value and a lower $HWHM_D$ value, the matrix graphitic planes contains a larger amount of defects than fibers ones and is less organized [6, 46], suggesting a higher sensitivity to oxidation, according to the works of Ehrburger *et al.* [54]. Besides, the in-plane coherence length L_a is greater for the fibers than for the matrix.

	A_e	$FWHM_D$	$HWHM_G$	I_D/I_G	L_a [48]
	°	cm^{-1}	cm^{-1}	-	nm
Fibers	0.8 ± 0.1	73.2 ± 1.5	24.7 ± 0.2	4.9 ± 0.2	8.3 ± 0.1
Matrix	13.9 ± 0.4	97.8 ± 1.6	32.3 ± 0.4	4.3 ± 0.1	6.9 ± 0.1

TABLE 1 – Fibers and matrix micro-textural and structural parameters obtained from PLOM technique and Raman spectroscopy.

3.2. Post-tests surface morphologies and volumic porous topologies

3.2.1. Oxidation morphologies and dominant reactive phase

Fig. 4 displays SEM micrographs of the C/C material constituants, *i.e.* fibers and matrix, at a pristine state and after oxidation under the three oxidizing atmospheres at the highest relative temperature.

Compared to the pristine state on Fig. 4a, the lengthwise matrix surface displays marks of oxidation under the three considered oxidizing atmospheres. One can notice that these oxidation patterns differ from an oxidative species to another. Whereas the matrix surface is pitted under O_2 on Fig. 4b, it displays a laminated appearance under H_2O on Fig. 4c and a dented one under CO_2 on Fig. 4d.

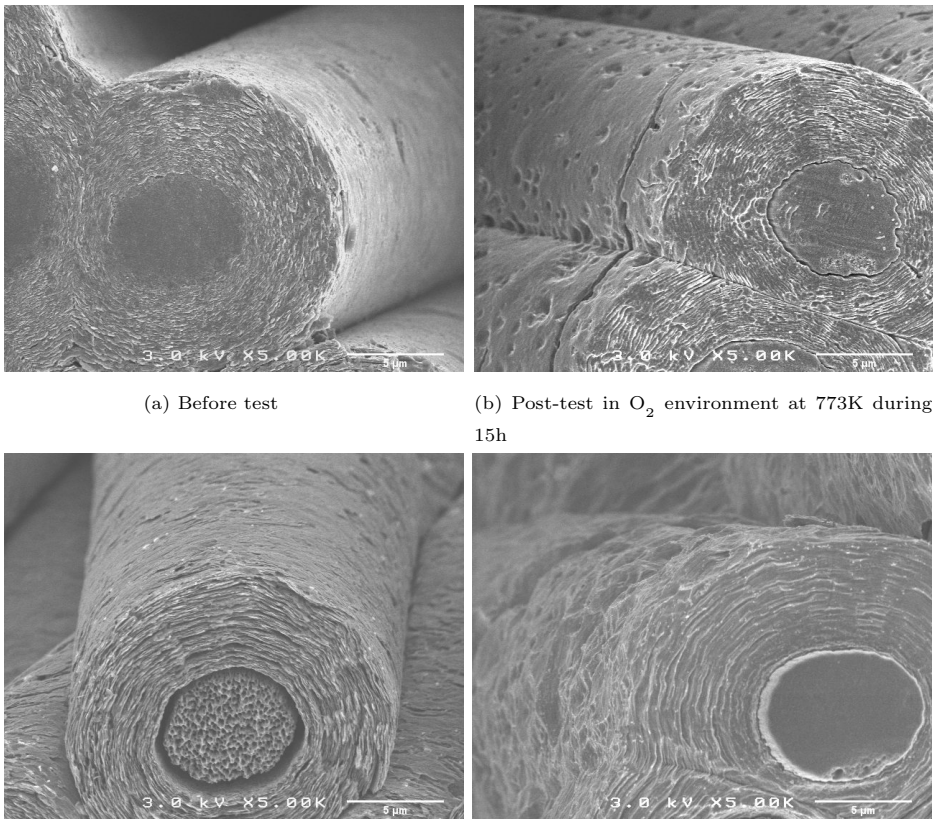

(a) Before test

(b) Post-test in O_2 environment at 773K during 15h

(c) Post-test in H_2O environment at 1223K during 15h

(d) Post-test in CO_2 environment at 1148K during 20h

FIGURE 4 – SEM images of the tip of a yarn from the C/C samples at different states : (a) before test ; post-test (b) under O_2 at 773K during 15h ; (c) under H_2O at 1223K during 15h ; under CO_2 at 1148K during 20h.

On the other hand, under O_2 and CO_2 atmospheres, fibers are stripped of the matrix on a small length because of their lower oxidation reactivity. Besides, they feature very few oxidation marks, except some pits at their extreme surface. This indicates that the matrix is the only reacting phase under O_2 and CO_2. Nevertheless, one has to exercise caution under H_2O because of the higher degradation at the tip of the fibers compared to the other atmospheres. Here, the exposed fiber sections seem to recede at least as much as the section of the matrix at the tip of the yarn. However, as it will be detailed in the following

section, the affected surface of the matrix is much larger than that of the fibers , because it does not only concern the tip of the yarns, but the entire porous volume of the material. Hence, the matrix overall reactivity in the porous material holds the dominant role.

3.2.2. Evolution of the volumic porous topology

Fig. 5 displays core slices of the pre-test µCT images and residues of oxidation for each of the oxidizing atmospheres at the highest relative temperature. White areas indicate the pristine material and the colored ones highlights the oxidized parts (*i.e.* the residues of oxidation). Residues are homogeneously spread all over the sample volume. Besides, Fig. 5 demonstrates that oxidation only affects the RL PyC matrix located in the open volume, *i.e.* the matrix covering the periphery of the yarns in the meso-scale pores and the one covering the fibers in the yarns in the micro-scale pores.

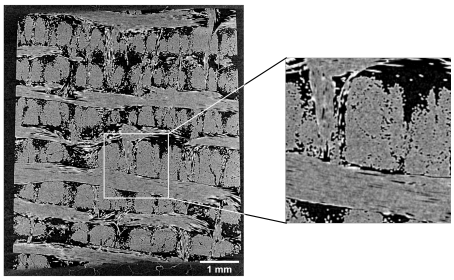

(a) Before test in O_2 environment

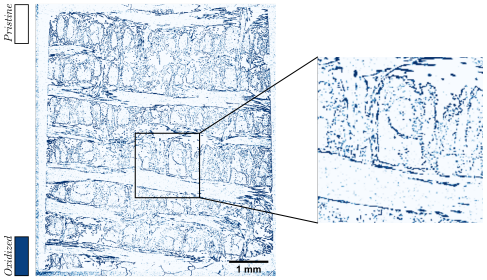

(b) Post-test residuals in O_2 environment at 773K

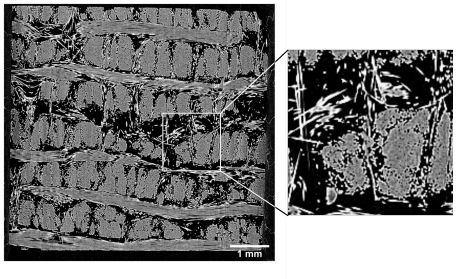

(c) Before test in H_2O environment

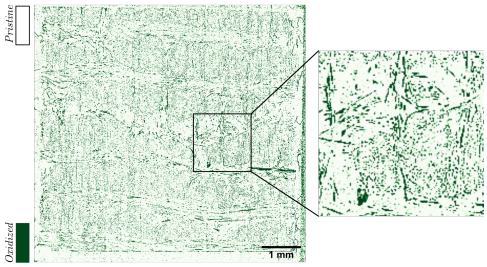

(d) Post-test residuals in H_2O environment at 1223K

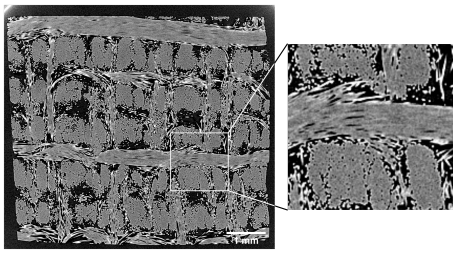

(e) Before test in CO_2 environment

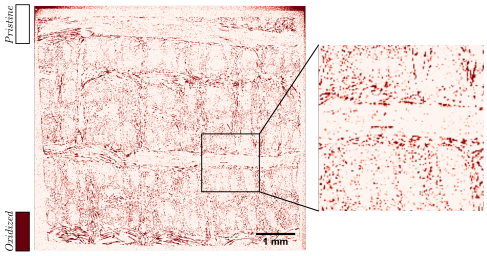

(f) Post-test residuals in CO_2 environment at 1148K

FIGURE 5 – Core slices of µCT images of the samples (a, c, e) at a pristine stage, and of the oxidation residuals on processed µCT images in (b) O_2-, (d) H_2O- and (f) CO_2-containing atmospheres at various temperatures.

The analysis of the volumic samples topologies at the highest test temperatures reveals the same behavior at the lowest temperatures. Thus, for each of the oxidation atmospheres and test temperatures, the matrix is the most reactive phase

and seems to be affected by oxidation throughout the whole sample volume.

3.3. Exploitation of the experimental oxidation activities

Graphs from Fig. 6 display raw oxidation results of the samples burn-off defined by Eq. 4. One can note the neat increase of mass loss with temperature under each atmosphere and the different activation temperatures according to the oxidation species.

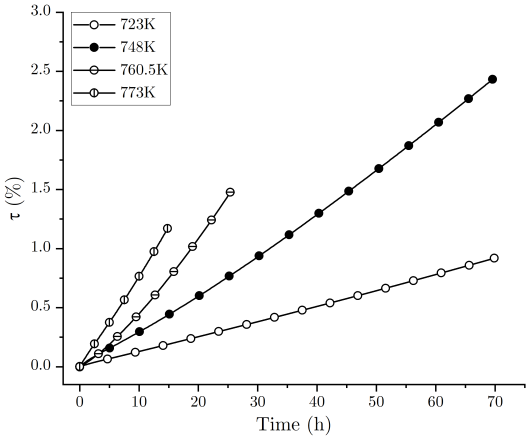

(a) O_2 environment

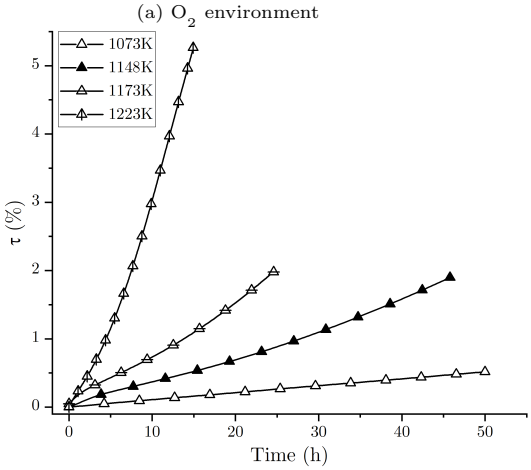

(b) H_2O environment

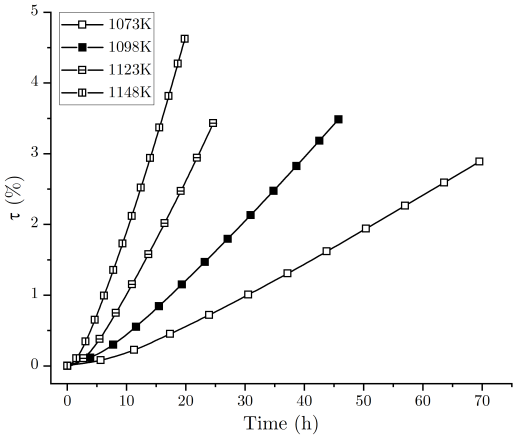

(c) CO_2 environment

FIGURE 6 – Burn-off evolution with time and temperature under (a) O_2-, (b) H_2O- and (c) CO_2-containing atmospheres.

The logarithm of the oxidation rate constant k for each oxidizing atmosphere, computed from Eq. 7, is reported on the Arrhenius-type plot of Fig. 7. A simple linear fitting is achieved on the three sets of data. According to Eq. 8, intercepts and slopes of the fitting curves give pre-exponential factors and activation energies, respectively. For the RL PyC matrix the values and the associated correlation coefficient r_c are indexed in Table 2.

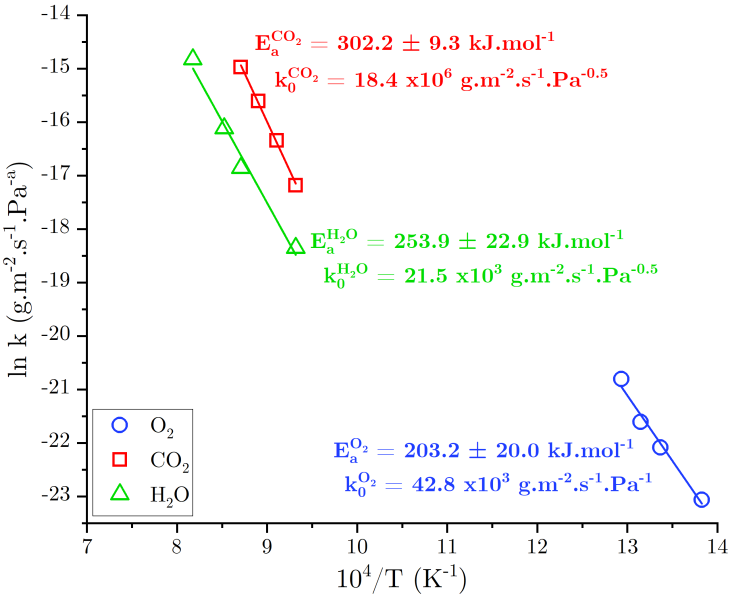

FIGURE 7 – Evolution of $ln\ k$ vs the inverse temperature in O_2-, H_2O- and CO_2-containing atmospheres and associated linear fit.

Thus, from activation energies values, the following ascending classification of the RL PyC matrix oxidation resistance is made : $O_2 < H_2O < CO_2$. However, considering the oxidation reactivities from Fig. 7 and the pre-exponential factors in Table 7, the RL PyC matrix seems more reactive under CO_2 than under H_2O.

Atmosphere		Temperature	k_0	E_a	r_c
		K	$g.m^{-2}.s^{-1}.Pa^{-a}$	$kJ.mol^{-1}$	-
$\mathbf{O_2}/N_2$	20/80	723 - 773	42.8×10^3	203.2 ± 20.0	0.9810
$\mathbf{H_2O}/N_2$	20/80	1073 - 1223	21.5×10^3	253.9 ± 22.9	0.9839
$\mathbf{CO_2}/N_2$	20/80	1073 - 1148	18.4×10^6	302.2 ± 9.3	0.9981

TABLE 2 – Pre-exponential factors and activation energies for the RL PyC matrix under O_2, H_2O and CO_2 atmospheres and associated correlation coefficient.

3.4. Proof of evidence of an oxidation reaction in chemical regime

To properly determine kinetics, oxidation tests have to be carried out in the chemical regime, at the surface of the material and also in its porous volume, avoiding any limitation by diffusion [10]. Such a precaution ensures the proper identification of the true kinetic parameters related to the intrinsic oxidation mechanism. In this section, the existence of a chemical regime at the surface and inside the porous volume of the material will be demonstrated using experiments and modeling. This aims at proving that the oxidation kinetics identified in Section 3.3 are indeed associated to the intrinsic behavior of the RL PyC matrix.

3.4.1. Chemical regime at the sample surface

The consumption ratio per geometrical surface unit ζ for each oxidizing experiment has been computed from Eq. 9. Its evolution with temperature and the type of oxidizing atmosphere is reported on Fig. 8. One can note that the consumption of the oxidizing atmosphere logically increases with temperature, but remains under a cut-off threshold ζ_{max} of 4.6 x10^{-3} %.mm^{-2} for each experiment. The study of Zancanaro *et al.* [38] carried out on the same TGA equipment as in this study proved that the ratio between the number of carbon moles consumed and the amount of available oxidizing species has to remain under 1% in the close environment of the sample geometric surface to ensure an oxidation reaction in chemical regime, which is equivalent to $\zeta_{max} = 4.6 \times 10^{-3}$ %.mm^{-2} for cubic samples of 6 mm edge length. Thus, ζ values from Fig. 8 provide evidence

of an established chemical regime at the samples surfaces.

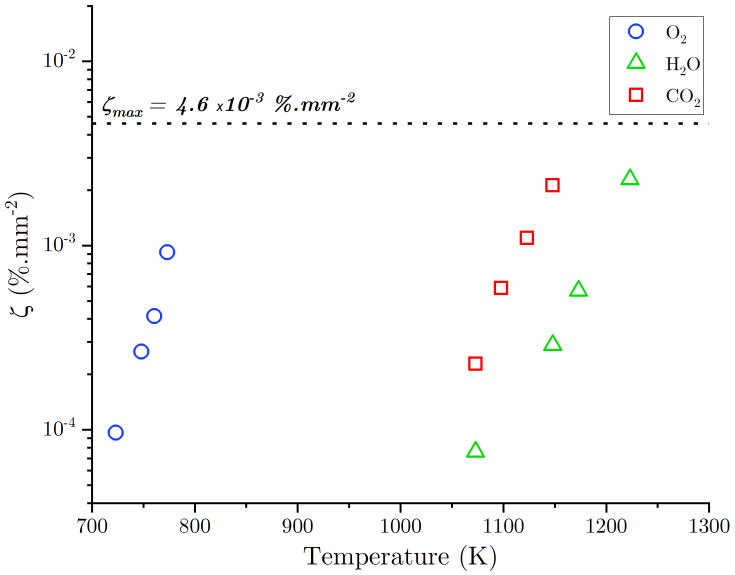

FIGURE 8 – Evolution of ζ with temperature in O_2-, H_2O- and CO_2-containing atmospheres.

3.4.2. Chemical regime in the sample volume

The experimental characterizations of the extent of oxidation throughout the porous volume in Section 3.2 have evidenced that the matrix covering the fibers, inside the yarns and at their periphery, is the dominant reacting phase and gets degraded uniformely no matter the depth inside the material.

This suggests that the chemical reaction rate is slower than the mass transport everywhere inside the porous medium. To confirm this, we provide computations of the Thiele modulus Θ at each temperature and under each oxidizing atmosphere, which gives an estimation of the competition between reaction and diffusion in a porous medium. A value below 1 denotes a chemical reaction-controlled regime where the speed of the diffusion of the oxidation gas is faster than the oxidation reaction (*i.e.* low temperatures). A value above 1 is an indicator of limitations by diffusion the speed of the oxidation reaction is faster than diffusion (*i.e.* high temperatures). It has been extensively defined for fibrous architectures [15, 37, 55, 56] and is applicable to a highly porous C/C

composite as the one of this study, where the matrix is the only reacting phase, without loss of precision. It is defined as follows :

$$\Theta = L\sqrt{\frac{\sigma_v k_{het,m}}{D_{\text{eff}}}} \tag{10}$$

where L is the characteristic length of the material which is taken equal to 3.10^{-3} m, *i.e.* the sample half-thickness, because it has been identified that oxidation took place through the whole bulk of the sample. The matrix heterogeneous reactivity $k_{het,m}$ (m.s^{-1}) is supposed to verify Eq. 8. The effective diffusion coefficient D_{eff} for an isotropic material of the type of the porous C/C composite of this study is defined as follows :

$$D_{\text{eff}} = D_0 \frac{\varepsilon^{1+\alpha}}{\eta} \tag{11}$$

where ε is the porosity of the C/C composite equal to 0.37, η is the tortuosity and α is a diffusion parameter depending on the direction of the fibrous architecture. The values for these parameters for the C/C composite of this study are given in the work of Charles *et al.* [52]. For the present calculations, they are averaged values of the X, Y, and Z directions and equal to 1.40 and 0.65 respectively. The binary diffusion coefficient D_0 ($\text{m}^2.\text{s}^{-1}$) of the oxidizing species in the gas mixture is computed from the recommended data from Massman [57] at each test temperature.

Fig. 9 sums up the Thiele modulus evolution with temperature for each oxidizing gas of this study. One can notice that Θ values are neatly below 1 (even < 0.5) for each of the oxidation tests. This confirms that a chemical reaction-controlled regime is reached everywhere in the porous volume. Besides, in addition to the SEM and 3D-image characterizations mentioned above, it also confirms that the oxidation reaction is homogeneous in the volume and only concerns the RL PyC matrix. This analysis strengthens the conclusion concerning the existence of a chemical reaction-controlled regime at the sample surface as well. Thus, oxidation kinetic parameters determined in Section 3.3 are proved to be intrinsic.

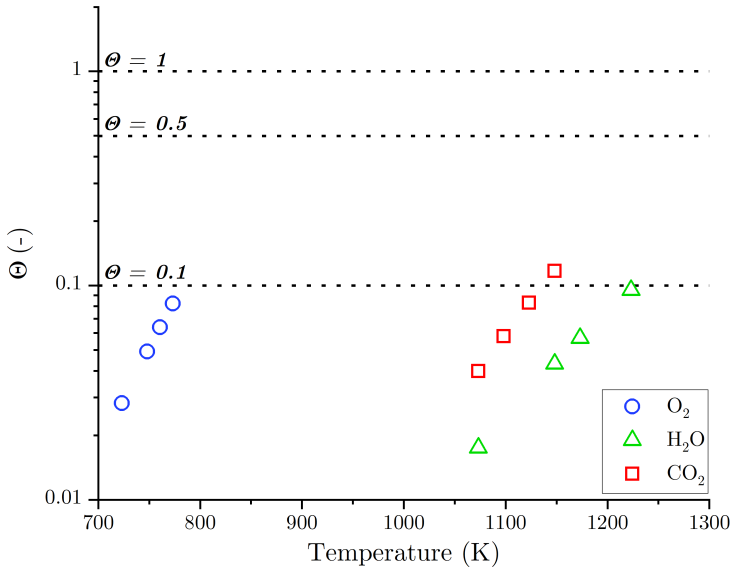

FIGURE 9 – Evolution of the Thiele modulus with temperature for the oxidation tests in the O_2-, H_2O- and CO_2-containing atmospheres.

3.5. Comparisons with literature data

Table 3 contains a brief summary of activations energies from this study compared to various data from literature in O_2, H_2O and CO_2-containing atmospheres collected on different types of carbonaceous materials. On the other hand, graphs from Fig. 10 allow visual comparison with some of the mentioned studies in Table 3, for which oxidation activities have been converted in the units and conditions of this study. These graphs are discussed in detail in the following sections.

3.5.1. In O_2-containing atmosphere

According to Fig. 10a, experimental oxidation data under dry air for the RL PyC matrix of this study are very well located among oxidation kinetics for other carbonaceous materials from other studies. In fact our data are well located whithin the bounds of Smith's data collected on various types of carbons up to 1650K. On the other hand, up to approximately 1250K, the oxidation activity of the RL PyC matrix of this study is located below the values reported by

Luo *et al.* [18] for a so-called ex-CVD matrix. Up to 1650K it is also located below the values of Bertran *et al.* [21] obtained for an ex-resin matrix, and up to approximately 3300K it is below the one of Drawin *et al.* [17] obtained on an ex-pitch matrix. It also exceeds the oxidation reactivity of graphite particles reported by Bradley *et al.* [20] above approximately 820K. Ehrburger *et al.* [54] and Lahaye *et al.* [58] made a strong correlation between the amounts of carbon defects and of active sites and reactivity. Thus, considering that the pyrolytic structure of an RL PyC matrix prepared by CVI features a lesser amount of in-plane defects, than an ex-resin, ex-pitch or an ex-CVD matrix, as suggested by the results in Table 1, the matrix of this study is expected to be less reactive. Actually, Bertran *et al.* [21] determined a $FWHM_D$ of 133 cm^{-1} for their ex-resin matrix, whereas the one for the RL PyC matrix of this study is 97.8 cm^{-1}, which denotes a lesser amount of in-plane defects. On the other hand, the RL PyC matrix structure might be less organized and display more in-plane defects than graphite particles, which explains the higher reactivity as compared to the data from Bradley *et al.* [20]. The relative value of the oxidation activity of the RL PyC matrix under dry air in comparison to other types of carbon on Fig. 10a is then in accordance with previous knowledge on the structure-reactivity relationship in dense carbons.

Ox. specie	Reference	E_a $kJ.mol^{-1}$	Carbonaceous material
O_2	Luo *et al.* [18]	121	C/C with ex-CVD matrix
	Bertran *et al.* [21]	122	ex-resin matrix
	Chang and Rusnak [12]	146 - 181	ground ex-resin C/C
	McKee [59]	146 - 188	C/C with ex-pitch matrix
	Smith [16]	179.4	various
	Dacic and Marinkovic [35]	184	ex-CVD matrix
	Rossberg [27]	209 - 243	spectroscopic carbon
	This study	203.2	ex-CVI RL PyC matrix
H_2O	Qin *et al.* [22]	157.0	ex-pitch matrix
	Qin *et al.* [22]	234.0	ex-PAN fibers
	Libby and Blake [19]	175.3	carbon particles
	Bradley *et al.* [20]	287.9	graphite particles
	Rossberg [27]	334.7	spectroscopic carbon
	This study	253.9	ex-CVI RL PyC matrix
CO_2	Ergun [26]	246.9	various activated carbons
	Bradley *et al.* [20]	284.9	graphite particles
	Golovina *et al.* [23]	313.8	graphites at LT
	Rossberg [27]	359.8	spectroscopic carbon
	Shelef and Walker [60]	364	spectroscopic graphite
	McKee *et al.* [24, 25]	386.3	isotropic carbon powder
	This study	302.2	ex-CVI RL PyC matrix

TABLE 3 – Activation energy data of various carbonaceaous material under O_2, H_2O and CO_2 oxidizing atmospheres from literature and this study. [*LT* meaning low temperatures.]

Regarding activation energies, a value of 179.4 kJ.mol^{-1} was found by Smith [16] for various carbonaceous materials under dry air, whereas one of 122 kJ.mol^{-1} for an ex-resin matrix was found by Bertran *et al.* [21] in dry air. Chang and Rusnak [12] and McKee [59] found quite the same range of activation energies of

146 to 181 kJ.mol for ground C/C composites filled with carbonaceous organic binders oxidized in dry air and 146 to 188 kJ.mol^{-1} for C/C composites made of a carbonized ex-pitch matrix. On the other hand, Dacic and Marinkovic [35] and Luo *et al.* [18] identified activation energies of 184 kJ.mol^{-1} and 121 kJ.mol^{-1} for two different ex-CVD matrices. The value identified in this study of 203.2 kJ.mol^{-1} rather matches with these data. These values are collected in Table 3.

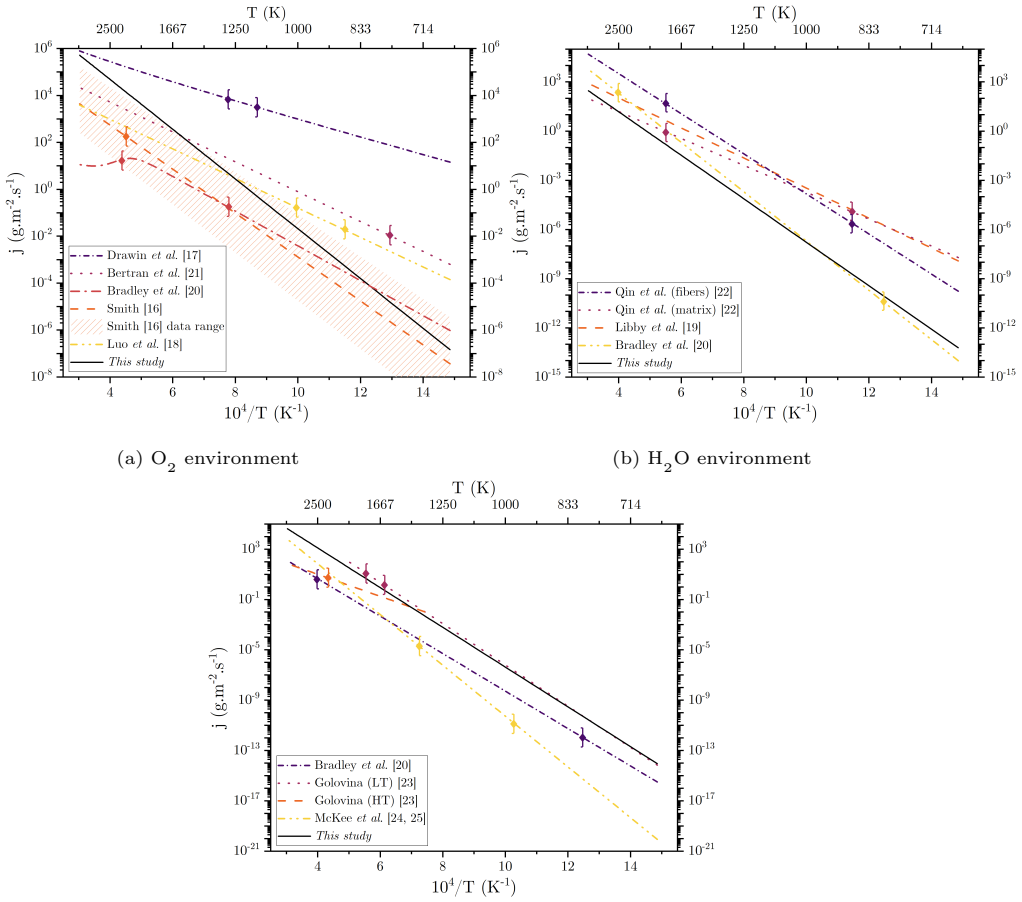

(a) O_2 environment

(b) H_2O environment

(c) CO_2 environment

FIGURE 10 – Comparison with literature data of the present oxidation results for a RL PyC matrix under (a) O_2-, (b) H_2O- and (c) CO_2-containing [16, 17, 18, 19, 20, 21, 22, 23, 24, 25]. [*LT* meaning low temperatures ; *HT* meaning high temperatures ; ♦ : bounds of the temperature domain.]

3.5.2. In H_2O-containing atmosphere

Fig. 10b displays the oxidation activity identified for the RL PyC matrix in a water vapor atmosphere in comparison with other data from literature. The corresponding Arrhenius curve is located below the one of an ex-resin matrix from the work of Qin *et al.* [22] up to 2500K. As kinetic data under water vapor are scarce, a comparison with the oxidation evolution of the ex-PAN fibers from

the above-mentioned work is also proposed. The Arrhenius curve of the the RL PyC matrix of this work is still located below. This indicates its better oxidation resistance. A good match is noticed with the oxidation activity of graphite particles from the work of Bradley *et al.* [20] : the oxidation activity of the RL PyC matrix is located above up to 950K denoting a somewhat lesser oxidation resistance.

In term of activation energy, the value identified for the RL PyC matrix in this study, which is of 253.9 kJ.mol^{-1}, is consistent with the one from the study of Bradley *et al.* [20] of 287.9 kJ.mol^{-1} on graphite particles, as already witnessed for oxidation in O_2. It also fits the value of 234 kJ.mol^{-1} for the ex-PAN fibers from the work of Qin *et al.* [22]. On the other hand, this value is much higher than the one identified for the ex-pitch matrix of the above-mentioned study accounting for 157 kJ.mol^{-1} and also indicating a lower oxidation sensitivity of the RL PyC matrix compared to less organized carbonaceous materials. Finally, Table 3 summarizes these data for a convenient comparison.

3.5.3. In CO_2-containing atmosphere

Similarly, the evolution of oxidation kinetics for the RL PyC matrix under a CO_2-containing atmosphere are in accordance with literature data as suggested by Fig. 10c with a clear insertion among data from literature identified on different types of graphitic carbons. One can notice that there is an especially good match with the data from Golovina [23] on graphites at low temperatures. The evolution of the mass loss rate associated to the RL PyC is also located above the ones from the works of Bradley *et al.* [20] and McKee *et al.* [24, 25] on graphites, confirming its lower oxidation resistance compared to highly organized materials.

Besides, the activation energy experimentally identified of 302.2 kJ.mol^{-1} is in line with the values of 284.9 and 313.8 kJ.mol^{-1} reported respectively by Bradley *et al.* [20] on graphite particles and Golovina [23] on graphites at low temperatures. McKee *et al.* [24, 25] determined a higher value of 386.3 kJ.mol^{-1} on isotropic carbon powders. Shelef and Walker [60] determined an activation energy

of 364 kJ.mol^{-1} for a spectroscopic graphite under a purified carbon dioxide atmosphere. On the other hand, Ergun [26] identified an activation energy of 246.9 kJ.mol^{-1} on various activated carbon materials.

3.6. Wide-ranging comparison

Finally, Table 3 displays a global trend of oxidation resistance based on activation energies between the three considered atmospheres which might be summed up as follows : $O_2 < H_2O < CO_2$. In particular, the work of Rossberg [27] that has established oxidation rate laws on the same carbonaceous material for the three oxidizing atmospheres is consistent with this classification, as well as the activation energies identified in this study for the RL PyC matrix.

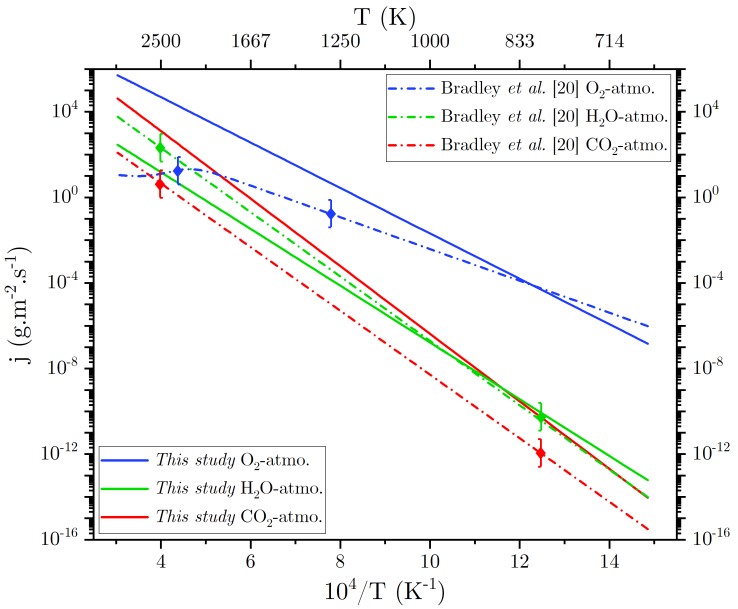

FIGURE 11 – Evolution of the oxidation activity for the graphite particles from Bradley *et al.* [20] and for the RL PyC matrix of this study under O_2-, H_2O- and CO_2-containing atmospheres. [♦ : bounds of the temperature domain.]

On the other hand, the higher resistance of the RL PyC matrix to H_2O than to CO_2 in this study, based on the oxidation reactivity values, has been mentioned above, but is not the trend which is commonly witnessed in literature. Walker *et al.* [10] reported experimental works in which the mass loss of a graphitized carbon rod was 2.8 times higher at 1373K in a water vapor environment than in a carbon dioxide atmosphere. Graphite particles reported in the work of Bradley *et al.* [20] remain more oxidation resistant in a CO_2 environment than in an H_2O atmosphere. Fig. 11 allows a visual comparison of all the data from this study in O_2-, H_2O- and CO_2-containing atmospheres with the ones from the work of Bradley *et al.* [20]. From Fig. 11, it is clear that in fact the RL PyC matrix of this study is more oxidation resistant to H_2O than to CO_2 up to approximately 870K considering the reaction oxidation activity.

From that point, the different trends observed in terms of oxidation reactivities and activation energies has to be contrasted.

First, activation energies cannot account by themselves for the overall oxidation behavior. The pre-exponential factor has to be considered as well. However, there is a great lack of information in literature for this parameter associated to the oxidation behavior of carbons under the considered atmospheres. This is the reason why the above classification based on activation energies is not representative of the reactivity for every type of carbon, but more importantly on a wide range of temperature. This is effectively demonstrated by Bradley *et al.* [20] on Fig. 11 : graphite particles become more resistant under O_2 than under CO_2 from 2120K whereas activation energies display an opposite behavior.

In the mean time, the nature of the oxidized carbonaceous material has to be considered. Data from Rossberg [27], Walker *et al.* [10] and Bradley *et al.* [20] were collected on spectroscopic carbons, graphitized carbons and graphite particles that are generally reported as highly organized and purified materials. The RL PyC matrix cannot be considered as such, considering its structure and texture features detailed in Section 3.1. Walker *et al.* [10] reported from different works that a retardation phenomenon under water vapor environment

caused by the chemisorption of hydrogen might happen. They also detailed that hydrogen chemisorption is strong and rapid, and is more likely to occur when the carbon surface displays heterogeneities, defects and impurities. That being said, the difference in the magnitude of oxidation reactivities under H_2O and CO_2 observed for the RL PyC matrix compared to highly organized carbons from the above-mentioned studies might then be explained by this retardation phenomenon, interpreted as the population of some of the carbon active sites, instead of being oxidized by H_2O. The two main sources of chemisorbed hydrogen atoms are : either a direct chemisorption of a hydrogen atom to a carbon site instead of forming $H_{2(g)}$ when $CO_{(g)}$ is released from the surface ; or the chemisorption of $H_{2(g)}$ coming from the gas phase after having been previously produced by H_2O reduction. Another side reaction reported by Walker *et al.* [10] is called the « water gas-shift reaction ». The reactant $H_2O_{(g)}$ may be consumed by the product $CO_{(g)}$ to form $CO_{2(g)}$ which reduces the $H_2O_{(g)}$ concentration in the close environment of the carbon surface. This side reaction is reported to be enhanced by the chemisorption of hydrogen atoms and by the nature of the carbonaceous material. Then, it can potentially contribute to invert the reaction magnitude ordering between H_2O and CO_2.

Finally, dissocation energies that have been cited before, and that follow the general trend of activation energies mentioned above, even for not highly organized materials, only account for the dissociation of an O-atom and a CO-molecule from the carbon surface. They do not include side reactions and for example the dissociation energy of the H-atom, which is also a product of the reaction of carbon with H_2O in the same molar proportion as CO according to Eq. 2. The cited dissocation energies are then insufficient to draw up a general classification of carbon oxidation resistance under the considered oxidizing environment.

4. Conclusions

The intrinsic kinetics parameter of an RL PyC matrix under three different oxidizing atmospheres, *i.e.* O_2, H_2O and CO_2, were identified throughout an

original method. A very porous C/C composite was considered, as the only way to study the oxidation behavior of a PyC material deposed by a CVI process on an ex-PAN fibrous architecture. The matrix has been proven to be the only reacting phase. The establishment of the oxidation reaction process in chemical regime at the surface and in the porous volume of the material, required to extract the intrinsic parameters of the matix, was proven with the means of experimental charaterizations and analytical modeling considerations. The identified kinetics values for the PyC material in question are brand new and are as follows : in O_2 the associated E_a is of 203.2 kJ.mol^{-1} and k_0 is equal to 42.8 x 10^3 g.m^{-2}.s^{-1}.Pa^{-1} ; in H_2O, E_a = 253.9 kJ.mol^{-1} and k_0 = 21.5 x 10^3 g.m^{-2}.s^{-1}.Pa$^{-0.5}$; and under CO_2, E_a = 302.2 kJ.mol^{-1} and k_0 = 18.4 x 10^6 g.m^{-2}.s^{-1}.Pa$^{-0.5}$. Comparisons with literature data collected over different types of carbonaceous materials were discussed and attested from the veracity and consistency of the results.

Similar experiments could be run on other types of pyrocarbons (regenerative laminar (ReL), smooth laminar (SL), isotropic (I)) in order to identify kinetic parameters related to their peculiar pyrolytic structure. On the other hand, reaction partial orders have been assumed so far. The identification of their actual values throughout similar experiments under different oxidizing species partial pressures could be an outlook of this work.

Acknowledgments

The authors wish to thank ArianeGroup SAS that have financially supported this work throughout a PhD grant to Marina Fradin. Olivier Caty (Bordeaux INP, LCTS) is warmly acknowledged for helping in 3D-images acquisition. X-ray µCT scans were acquired at the *Placamat* characterization service unit of Bordeaux University and CNRS.

Nomenclature

Symbol	Meaning	Unit(s)
Greek symbols		
L	Characteristic length of the material	m
α	Diffusion parameter (Eq. 11)	-
η	Tortuosity	-
τ	Burn-off	%
$\dot{\tau}$	Burn-off rate	%.s^{-1}
Θ	Thiele modulus	-
σ_v	Effective surface area	m^{-1}
ζ	Consumption ratio per geometrical surface unit	%.mm^{-2}
Latin symbols		
a	Reaction partial order	-
A_e	Extinction angle	$^\circ$
D_0	Binary diffusion coefficient	m^2.s^{-1}
D_{eff}	Effective diffusion coefficient	m^2.s^{-1}
E_a	Activation energy	J.mol^{-1}
$FWHM_D$	Full Width at Half Maximum of the D-band	cm^{-1}
$HWHM_G$	Half Width at Half Maximum of the G-band	cm^{-1}
I_D/I_G	Intensity ratio of the D- and G-bands	-
j	Oxidation activity	g.m^{-2}.s^{-1}
k	Oxidation reactivity	g.m^{-2}.s^{-1}.Pa^{-a}
$k_{het,m}$	Matrix heterogeneous reactivity	m.s^{-1}
k_0	Pre-exponential factor	g.m^{-2}.s^{-1}.Pa^{-a}
L_a	In-plane coherence length	nm
m	Mass	g
n_C^{cons}	Consumed carbon moles	mol
n_{ox}^{cons}	Available oxygen moles	mol
P_{ox}	Partial pressure	atm
$\mathcal{R}$	Universal ideal gas constant	J.mol^{-1}.K^{-1}
r_c	Correlation coefficient	-
S_{geo}	Geometrical surface	mm^2
S_{vol}	Internal surface	m^2
t	Time	s
T	Temperature	K
V_{geo}	Geometrical volume	m^3
Subscripts and superscripts		
$_0$	Relative to initial state	-
$_i$	Relative to the instant i	-

Data availability

The raw data required to reproduce these findings cannot be shared at this time due to legal reasons. The processed data required to reproduce these findings cannot be shared at this time due to legal reasons.

References

[1] R. Naslain, F. Langlais, R. Fedou, The CVI-processing of ceramic matrix composites, Journal de Physique Colloques 50 (C5) (1989) C5–191–C5–207. doi:10.1051/jphyscol:1989526.

[2] N. P. Padture, Advanced structural ceramics in aerospace propulsion, Nature Materials 15 (8) (2016) 804–809. doi:10.1038/nmat4687.

[3] E. Fitzer, L. M. Manocha, Carbon Reinforcements and Carbon/Carbon Composites, Springer, 1998. doi:10.1007/978-3-642-58745-0.

[4] X. Jin, X. Fan, C. Lu, T. Wang, Advances in oxidation and ablation resistance of high and ultra-high temperature ceramics modified or coated carbon/carbon composites, Journal of the European Ceramic Society 38 (1) (2018) 1–28. doi:10.1016/j.jeurceramsoc.2017.08.013.

[5] C. Zweben, Chapter 10 - Composite Materials, in : M. Kutz (Ed.), Mechanical Engineers' Handbook, 4th Edition, 2015, pp. 1–37. doi:https://doi.org/10.1002/9781118985960.meh110.

[6] P. Morgan, Carbon fibers and their composites, 1st Edition, Taylor and Francis, Boca Raton, FL, 2005. doi:10.1007/978-94-017-9478-7_5.

[7] V. Borie, Y. Maisonneuve, D. Lambert, G. Lengellé, Ablation des matériaux de tuyères de propulseurs à propergol solide, Technical report 13, ISSN-0078-3781 (1990).

[8] G. Duffa, Ablative Thermal Protection Systems Modeling, AIAA Education Series, 2013. doi:10.2514/4.101717.

[9] G. L. Vignoles, J. Lachaud, Y. Aspa, Environmental Effects : Ablation of C/C Materials-Surface Dynamics and Effective Reactivity, in : Ceramic Matrix Composites, John Wiley & Sons, Inc., Hoboken, NJ, USA, 2014, Ch. 12, pp. 353–388. doi:10.1002/9781118832998.ch12.

[10] P. L. Walker, F. Rusinko, L. G. Austin, Gas reactions of carbon, Advances in Catalysis Volume 11 (1959) 133–221. doi:https://doi.org/10.1016/S0360-0564(08)60418-6.

[11] E. Duvivier, Cinétique d'oxydation d'un composite Carbone/Carbone et influence sur le comportement mécanique, Ph.D. thesis, Bordeaux (1997). URL https://www.theses.fr/1997BOR10539

[12] H.-W. Chang, R. M. Rusnak, Oxidation behavior of carbon-carbon composites, Carbon 17 (5) (1979) 407–410. doi:10.1016/0008-6223(79)90056-3.

[13] S. Kumar, J. Kushwaha, S. Mondal, A. Kumar, R. K. Jain, G. Rohini Devi, Fabrication and ablation testing of 4D C/C composite at 10MW/m2 heat flux under a plasma arc heater, Materials Science and Engineering A 566 (2013) 102–111. doi:10.1016/j.msea.2012.12.059.

[14] J. Lachaud, Y. Aspa, G. L. Vignoles, Analytical modeling of the steady state ablation of a 3D C/C composite, International Journal of Heat and Mass Transfer 51 (9-10) (2008) 2614–2627. doi:10.1016/j.ijheatmasstransfer.2008.01.008.

[15] G. L. Vignoles, A. Turchi, D. Bianchi, P. Blaineau, X. Lamboley, D. Le Quang Huy, et al., Ablative and catalytic behavior of carbon-based porous thermal protection materials in nitrogen plasmas, Carbon 134 (2018) 376–390. doi:10.1016/j.carbon.2018.03.087.

[16] I. W. Smith, The intrinsic reactivity of carbons to oxygen, Fuel (1978). doi:10.1016/0016-2361(78)90055-8.

[17] S. Drawin, M. Bacos, J. Dorvaux, Oxidation Model for Carbon-Carbon Composites, AIAA Journal AIAA-92-50 (1992) 0–9. doi:10.2514/6.1992-5016.

[18] R. Luo, J. Cheng, T. Wang, Oxidation behavior and protection of carbon/carbon composites prepared using rapid directional diffused CVI techniques, Carbon 40 (11) (2002) 1965–1972. doi:10.1016/S0008-6223(02)00025-8.

[19] P. A. Libby, T. R. Blake, Burning carbon particles in the presence of water vapor, Combustion and Flame 41 (C) (1981) 123–147. doi:10.1016/0010-2180(81)90047-X.

[20] D. Bradley, G. Dixon-Lewis, S. El-din Habik, E. M. Mushi, The oxidation of graphite powder in flame reaction zones, Symposium (International) on Combustion 20 (1) (1984) 931–940. doi:10.1016/S0082-0784(85)80582-8.

[21] X. Bertran, G. Chollon, J. Dentzer, R. Gadiou, S. Fouquet, M. A. Dourges, et al., Oxidation behavior at moderate temperature under dry and wet air of phenolic resin-derived carbon, Thermochimica Acta 649 (2017) 13–21. doi:10.1016/j.tca.2016.12.013.

[22] F. Qin, L. Na Peng, G. Qiang He, J. Li, Y. Yan, Oxidation kinetics and mechanisms of carbon/carbon composites and their components in water vapour at high temperatures, Corrosion Science 90 (2015) 340–346. doi:10.1016/j.corsci.2014.10.027.

[23] E. Golovina, The gasification of carbon by carbon dioxide at high temperatures and pressures, Carbon 18 (3) (1980) 197–201. doi:https://doi.org/10.1016/0008-6223(80)90061-5.

[24] D. W. McKee, Catalytic effects of alkaline earth carbonates in the carbon-carbon dioxide reaction, Fuel 59 (5) (1980) 308–314. doi:https://doi.org/10.1016/0016-2361(80)90215-X.

[25] D. McKee, Gasification of graphite in carbon dioxide and water vapor—the catalytic effects of alkali metal salts, Carbon 20 (1) (1982) 59–66. doi:https://doi.org/10.1016/0008-6223(82)90075-6.

[26] S. Ergun, Kinetics of the reaction of carbon with carbon dioxide, The Journal of Physical Chemistry 60 (4) (1956) 480–485. doi:10.1021/j150538a022.

[27] M. Rossberg, Experimentelle Ergebnisse über die Primärreaktionen bei der Kohlenstoffverbrennung, Zeitschrift für Elektrochemie, Berichte der Bunsengesellschaft für physikalische Chemie 60 (9-10) (1956) 952–956. URL http://onlinelibrary.wiley.com/doi/10.1002/bbpc.19560600905/abstract

[28] S. R. Kelemen, H. Freund, A comparison of O2 and CO2 oxidation of glassy carbon surfaces, Carbon 23 (6) (1985) 723–729. doi:10.1016/0008-6223(85)90234-9.

[29] O. Karlström, A. Brink, M. Hupa, Desorption kinetics of CO in char oxidation and gasification in O2, CO2 and H2O, Combustion and Flame 162 (3) (2015) 788–796. doi:10.1016/j.combustflame.2014.08.010.

[30] I. Golecki, Rapid vapor-phase densification of refractory composites, Materials Science and Engineering : R : Reports 20 (2) (1997) 37–124, r20. doi:https://doi.org/10.1016/S0927-796X(97)00003-X.

[31] D. Kopeliovich, 5 - Advances in manufacture of ceramic matrix composites by infiltration techniques, in : I. Low (Ed.), Advances in Ceramic Matrix Composites, second edition Edition, Woodhead Publishing Series in Composites Science and Engineering, Woodhead Publishing, 2018, pp. 93–119. doi:https://doi.org/10.1016/B978-0-08-102166-8.00005-0.

[32] Y. Xu, Chemical Vapour Infiltration, Springer London, London, 2010, pp. 165–213. doi:10.1007/978-1-84882-894-0_5.

[33] F. Langlais, G. Vignoles, 5.4 chemical vapor infiltration processing of ceramic matrix composites, in : P. W. Beaumont, C. H. Zweben (Eds.), Comprehensive Composite Materials II, Elsevier, Oxford, 2018, pp. 86–129. doi:https://doi.org/10.1016/B978-0-12-803581-8.03912-6.

[34] G. Vignoles, 8 - Chemical Vapor Deposition/Infiltration Processes for Ceramic Composites, in : P. Boisse (Ed.), Advances in Composites Manufacturing and Process Design, Woodhead Publishing, 2015, pp. 147–176. doi:https://doi.org/10.1016/B978-1-78242-307-2.00008-7.

[35] B. Dačić, S. Marinković, Kinetics of air oxidation of unidirectional carbon fibres/ CVD carbon composites, Carbon 25 (3) (1987) 409–415. doi:10.1016/0008-6223(87)90012-1.

[36] K. Z. Li, X. T. Shen, H. J. Li, S. Y. Zhang, T. Feng, L. L. Zhang, Ablation of the carbon/carbon composite nozzle-throats in a small solid rocket motor, Carbon 49 (4) (2011) 1208–1215. doi:10.1016/j.carbon.2010.11.037.

[37] J. C. Ferguson, F. Panerai, J. Lachaud, A. Martin, S. C. Bailey, N. N. Mansour, Modeling the oxidation of low-density carbon fiber material based on micro-tomography, Carbon 96 (2016) 57–65. doi:10.1016/j.carbon.2015.08.113.

[38] M. Zancanaro, N. Bertrand, F. Rebillat, Definition of Optimized Conditions to Extract Accurate Kinetic Laws from TGA Experiments : Modeling and Validation, Oxidation of Metals 87 (3-4) (2017) 393–402. doi:10.1007/s11085-017-9716-6.

[39] F. Panerai, T. Cochell, A. Martin, J. D. White, Experimental measurements of the high-temperature oxidation of carbon fibers, International Journal of Heat and Mass Transfer 136 (2019) 972–986. doi:10.1016/j.ijheatmasstransfer.2019.03.018.

[40] A. Lacombe, M. Lacoste, T. Pichon, 3D Novoltex® and Naxeco® carbon-carbon nozzle extensions ; matured, industrial and available technologies

to reduce programmatic and technical risks and to increase performance of launcher upper stage engines, 44th AIAA/ASME/SAE/ASEE Joint Propulsion Conference and Exhibit (July) (2008) 1–10. doi:10.2514/6.2008-5236.

[41] A. Lacombe, T. Pichon, J. M. Amouroux, HERAKLES thermal-structural composite materials boost rocket nozzle performance, 49th AIAA/ASME/SAE/ASEE Joint Propulsion Conference 1 PartF (July) (2013). doi:10.2514/6.2013-3863.

[42] E. Frank, L. M. Steudle, D. Ingildeev, J. M. Spörl, M. R. Buchmeiser, Carbon fibers : Precursor systems, processing, structure, and properties, Angewandte Chemie - International Edition 53 (21) (2014) 5262–5298. doi:10.1002/anie.201306129.

[43] C. Charles, Relations entre la structure de milieux fibreux et leurs propriétés thermiques et de transfert de masse, Ph.D. thesis, Université de Bordeaux (2022).
URL https://www.theses.fr/2021BORD0322

[44] A. P. Gillard, G. Couégnat, O. Caty, A. Allemand, P. Weisbecker, G. L. Vignoles, A quantitative, space-resolved method for optical anisotropy estimation in bulk carbons, Carbon 91 (2015) 423–435. doi:10.1016/j.carbon.2015.05.005.

[45] P. Lespade, A. Marchand, M. Couzi, F. Cruege, Caractérisation de matériaux carbonés par microspectrométrie Raman, Carbon 22 (4-5) (1984) 375–385. doi:10.1016/0008-6223(84)90009-5.

[46] J. M. Vallerot, X. Bourrat, A. Mouchon, G. Chollon, Quantitative structural and textural assessment of laminar pyrocarbons through Raman spectroscopy, electron diffraction and few other techniques, Carbon 44 (9) (2006) 1833–1844. doi:10.1016/j.carbon.2005.12.029.

[47] G. L. Vignoles, P. Weisbecker, J.-M. Leyssale, S. Jouannigot, G. Chollon, Carbones pyrolytiques ou pyrocarbones : des matériaux multiéchelles et multiperformances, Techniques de l'ingénieur 33 (2015). doi:10.51257/a-v1-nm3150.

[48] P. Mallet-Ladeira, P. Puech, C. Toulouse, M. Cazayous, N. Ratel-Ramond, P. Weisbecker, et al., A Raman study to obtain crystallite size of carbon materials : A better alternative to the Tuinstra-Koenig law, Carbon 80 (1) (2014) 629–639. doi:10.1016/j.carbon.2014.09.006.

[49] J. R. Arthur, Reactions between carbon and oxygen, Transactions of the Faraday Society 47 (1950) 164–178. doi:10.1039/tf9514700164.

[50] J. M. Calo, M. T. Perkins, A heterogeneous surface model for the "steady-state" kinetics of the Boudouard reaction, Carbon 26 (3) (1987) 395–407.

[51] J. Schindelin, I. Arganda-Carreras, E. Frise, V. Kaynig, M. Longair, T. Pietzsch, et al., Fiji : An open-source platform for biological-image analysis, Nature methods 9 (2012) 676–82. doi:10.1038/nmeth.2019.

[52] C. Charles, C. Descamps, G. L. Vignoles, Low pressure gas transfer in fibrous media with progressive infiltration : correlation between different transfer modes, International Journal of Heat and Mass Transfer 182 (2022) 121954. doi:10.1016/j.ijheatmasstransfer.2021.121954.

[53] G. Dupupet, Fibres de carbone, Techniques de l'ingénieur TIB625. (am5134) (2008) 19. doi:10.51257/a-v1-am5134.

[54] P. Ehrburger, F. Louys, J. Lahaye, The concept of active sites applied to the study of carbon reactivity, Carbon 27 (3) (1989) 389–393. doi:10.1016/0008-6223(89)90071-7.

[55] F. Panerai, A. Martin, N. N. Mansour, S. A. Sepka, J. Lachaud, Flow-tube oxidation experiments on the carbon preform of a phenolic-impregnated carbon ablator, Journal of Thermophysics and Heat Transfer 28 (2) (2014) 181–190. doi:10.2514/1.T4265.

[56] J. Lachaud, N. Bertrand, G. L. Vignoles, G. Bourget, F. Rebillat, P. Weisbecker, A theoretical/experimental approach to the intrinsic oxidation reactivities of C/C composites and of their components, Carbon 45 (14) (2007) 2768–2776. doi:10.1016/j.carbon.2007.09.034.

[57] W. J. Massman, A review of the molecular diffusivities of H2O, CO2, CH4, CO, O3, SO2, NH3, N2O, NO, and NO2 in air, O2 and N2 near STP, Atmospheric Environment 32 (6) (1998) 1111–1127. doi:10.1016/S1352-2310(97)00391-9.

[58] J. Lahaye, F. Louys, P. Ehrburger, The reactivity of carbon-carbon composites, Carbon 28 (1) (1990) 137–141. doi:10.1016/0008-6223(90)90104-7.

[59] D. W. McKee, Oxidation behavior and protection of carbon/carbon composites, Carbon 25 (4) (1987) 551–557. doi:10.1016/0008-6223(87)90197-7.

[60] M. Shelef, P. Walker, Transient phenomena in the gasification of graphite by high-purity carbon dioxide, Carbon 5 (2) (1967) 93–105. doi:https://doi.org/10.1016/0008-6223(67)90063-2.